Composites: Part A 84 (2016) 482–489

Contents lists available at ScienceDirect

Composites: Part A

journal homepage: www.elsevier.com/locate/compositesa

Electrophoretic deposition of aramid nanofibers on carbon fibers for highly enhanced interfacial adhesion at low content

Jea Uk Lee [a], Byeongho Park [b], Byeong-Su Kim [b], Dae-Ryung Bae [c,d], Wonoh Lee [e,*]

[a] Center for Carbon Resources Conversion, Korea Research Institute of Chemical Technology (KRICT), 141 Gajeong-ro, Yuseong-gu, Daejeon 34114, South Korea
[b] Department of Energy Engineering and Department of Chemistry, Ulsan National Institute of Science and Technology (UNIST), Ulsan 44919, South Korea
[c] Composites Research Division, Korea Institute of Materials Science (KIMS), 797 Changwon-daero, Changwon, Gyungnam 51508, South Korea
[d] University of Science and Technology, 217 Gajeong-ro, Yuseong-gu, Daejeon 34113, South Korea
[e] School of Mechanical Engineering, Chonnam National University, 77 Yongbong-ro, Buk-gu, Gwangju 61186, South Korea

ARTICLE INFO

Article history:
Received 12 November 2015
Received in revised form 5 February 2016
Accepted 26 February 2016
Available online 5 March 2016

Keywords:
A. Aramid fibers
B. Fiber/matrix bond
B. Interface/interphase
Electrophoretic deposition

ABSTRACT

Here, an anodic electrophoretic deposition was adopted to facilitate the large-scale uniform coating of nano-fillers onto carbon fibers to enhance the interfacial properties between carbon fibers and epoxy matrix. As interface–reinforcing materials, aramid nanofibers were introduced because of their superior mechanical properties and epoxy matrix-friendly functional groups. Furthermore, aramid nanofibers can be readily coated on carbon fibers via electrophoretic deposition because they are negatively-charged in solution with high electrical mobility. Finally, aramid nanofiber-coated carbon fibers showed significantly improved interfacial properties such as higher surface free energy and interfacial shear strengths (39.7% and 34.9% increases, respectively) than those of a pristine carbon fiber despite a very small amount of embedding (0.025 wt% of aramid nanofibers in a carbon fiber), and the short beam strength of the laminated composite prepared with the aramid nanofiber-coated carbon fibers was also improved by 17.0% compared to a non-modified composite.

1. Introduction

Advanced structural fibers such as carbon, glass, and aramid fibers have been intensively adopted in high-performance application fields, including aviation, aerospace, automotive, shipbuilding, sports, and military [1–4]. To meet industrial requirements with a high specification, many efforts have focused on improving the material properties of each component comprising fiber-reinforced composites [5]. Besides the well-designed combination of reinforcing fibers and polymer matrix, the highly adhesive interface between fibers and matrix is also a crucial factor to achieve the ideal performance of fiber-reinforced composites. For achieving better performance of structural composite parts, the control of the interfacial properties between fibers and matrix has been made toward higher adhesive strength, which can effectively help transfer an external load from the matrix to fiber reinforcements [6,7]. Therefore, many approaches have been reported to enhance fiber–matrix interfacial properties, such as modifying conventional sizing agents, increasing the chemical functionality of fiber-surface, or enlarging effective interfacial area [8–10]. To obtain higher adhesive strength, conventional sizing agents have been modified by hybridizing with reinforcing carbon nano-fillers such as carbon nanofibers, carbon nanotubes, graphene sheets, and their hybrids [11–13], or carbon nanotubes have been vertically grown on fiber surfaces to increase effective interfacial area [8]. Besides adopting as structural reinforcing fillers, carbon nanomaterials can be further applied for energy, environment, and biological areas as key building blocks to produce various and complex geometry [14].

Aramid fibers (also known as Kevlar) have outstanding mechanical properties such as high modulus, and high tenacity at a significant low density, which have been regarded as an ideal reinforcing materials in advanced composites [15,16]. Recently, the nano-sized form of aramid fibers has been developed with maintaining great mechanical properties similar to their original macro-fibers [17]. Because a stable dispersion of aramid nanofibers (ANFs) is easily obtained in dimethyl sulfoxide (DMSO), their hybrids with carbon nanomaterials such as carbon nanotubes and graphene sheets have been successfully manufactured and embedded as fillers in polymeric composites to increase mechanical stiffness [18–21]. As a sizing material on reinforcing fibers, ANFs have been coated on

* Corresponding author at: School of Mechanical Engineering, Chonnam National University, 77 Yongbong-ro, Buk-gu, Gwangju 61186, South Korea. Tel.: +82 62 530 1682.
E-mail address: wonohlee@jnu.ac.kr (W. Lee).

http://dx.doi.org/10.1016/j.compositesa.2016.02.029
1359-835X/

glass fibers with graphene oxide using a layer-by-layer (LbL) assembly technique [22]. Even though surface free energy and interfacial shear strength have been successfully increased and tuned by altering layer architecture, the amount of coated-ANFs was not enough to cover the entire surface of fibers. In order to obtain the large amount of coated materials, the LbL method requires repetitive coating steps and counter-charged nanoparticles or polyelectrolytes, which can be undesirable to show the best performance of composites.

An electrophoretic deposition (EPD) is a simple and cost-effective process with considerable flexibility to coat on any electrically conducting substrates [23,24]. Due to the massive and rapid movement of charged nano-materials under an external electric field, it is possible to produce a large scale nano-structure on a substrate with only one-step coating. In this work, a simple anodic EPD was used to produce ANF-coated carbon fibers with improved interfacial properties (Fig. 1). In DMSO solution, ANFs are well-dispersed with negative surface charges. Therefore, by applying an electric field between electrodes, the negatively charged ANFs are attracted toward an anode and then can be readily deposited on carbon fibers without any chemical treatment and other unwanted materials. By varying the concentration of ANF suspensions under a certain EPD condition (voltage and time), the coating morphology and amount of ANFs can be controlled to obtain the best performance of carbon fiber-reinforced composites.

2. Experimental

2.1. Synthesis of ANFs

ANFs were prepared by following the method as reported by Yang et al. [17] and all reagents were purchased from Sigma–Aldrich. 0.25 g of chopped (~5.0 mm) Kevlar threads (Dupont) were added to 500.0 mL of dimethyl sulfoxide (DMSO) with 1.5 g of potassium hydroxide (KOH), and the solution was magnetically stirred for one week at room temperature, yielding an orange colored ANF suspension (0.05 wt%) in DMSO. In order to perform EPD, more suspensions were manufactured using the same method and 3.5 L of ANF solution was used in EPD.

2.2. Anodic EPD

In EPD stage, the anodic EPD was carried out with an ANF suspension. Here, four different concentrations of the ANF solution (C_i) were considered as 1.0×10^{-3}, 5.0×10^{-3}, 1.0×10^{-2}, and 5.0×10^{-2} wt%. Fourteen woven fabrics (80 × 80 mm, areal density = 22 mg/cm^2) of the carbon fibers (TR30, Mitsubishi) and fifteen 1.0 mm-thick stainless steel plates were sequentially connected to anodes and cathodes of the power supply (6035A System DC Power Supply, Agilent Technologies), respectively. Each fabrics and steel plates were placed with 5.0 mm of facing-distance in a fixture. In order to achieve a uniform electrical field, a conductive copper tape was applied to four edges of a carbon fabric so that uniform deposition can be obtained. EPD was performed under a constant voltage of 5.0 V for 1 min and the total amount of the ANF solution was 3.5 L (3,850 g). After EPD, ANF-coated carbon fibers were dried in 120 °C for 24 h.

2.3. Sample preparation of laminated composites

As for the preparation of carbon fiber composite samples, fourteen layers of the ANF-coated carbon fabric were laminated and a diglycidyl ether of bisphenol-A type epoxy resin (YD-128, Kukdo Chemicals) was injected with am anhydride curing agent (KBH-1089, Kukdo Chemicals) by a vacuum-assisted resin transfer molding process. The weight ratio of the epoxy resin and the curing agent was 10:9 (150 and 135 g). The composite samples were cured at 120 °C for 2 h. Note that all manufactured composite samples had similar thickness of 3.3 mm (±0.02 mm).

2.4. Measurement of surface free energy (SFE)

SFE of ANF-coated carbon fibers was measured from an advancing contact angle by the Wilhelmy method (K100SF tensiometer, Krüss). Five individual fibers (5.0 mm length) were placed parallel to each other (1.0 mm distance) onto a platinum holder and a contact rate was 0.005 mm/s. To determine polar and dispersive components of SFE, purified water and diiodomethane (158,429, Sigma

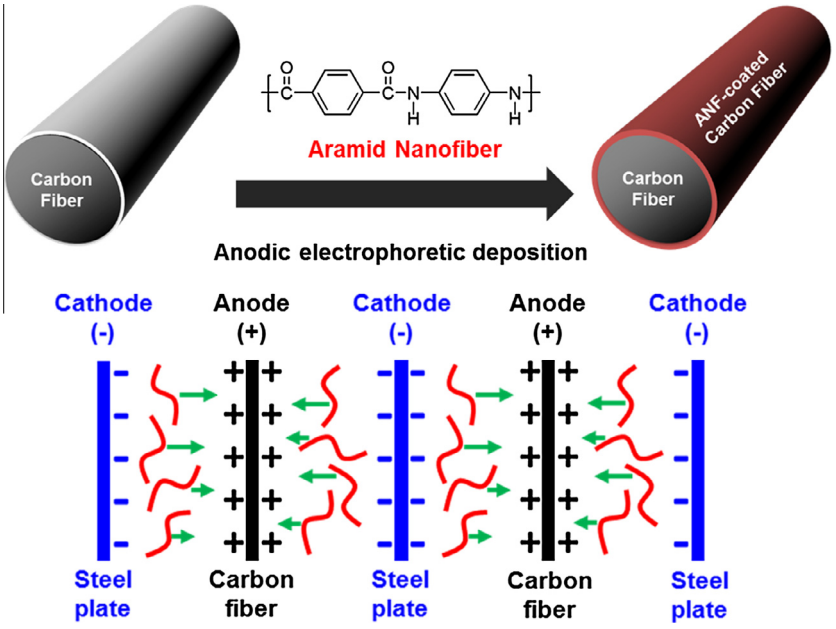

Fig. 1. Schematic illustration of coating of aramid nanofibers on carbon fiber surfaces by anodic electrophoretic deposition. (For interpretation of the references to color in this figure legend, the reader is referred to the web version of this article.)

Aldrich) were used as probe liquids, and the Owens–Wendt equation was used [25].

$$W_a = \gamma_L(1+\cos\theta) = 2\sqrt{\gamma_S^p\gamma_L^p} + 2\sqrt{\gamma_S^d\gamma_L^d} \quad (1)$$

where W_a is the work of adhesion, γ is the surface energy, and θ is the contact angle, respectively. The subscripts L and S are corresponding to testing liquids and a solid (a carbon fiber), and the superscripts p and d mean polar and dispersive components, respectively.

2.5. Measurements of interfacial shear strength (IFSS) and short beam strength (SBS)

IFSS between the ANF-coated fiber and epoxy resin was measured by the micro-droplet pull-out test [26]. A testing single fiber was held to a paper window frame with 10.0 mm width and 25.0 mm length. One micro-droplet of epoxy resin mixed with a curing agent at a weight ratio of 10:9, was applied to the fiber in the quarter length of the window-frame using the tip of a carbon fiber. The single carbon fiber with the epoxy droplet was cured at 120 °C for 2 h. After finishing the curing of the micro-droplet, the embedded fiber length (L_e) was measured using an optical microscope (LV100POL, Nikon). The fiber was then carefully cut from the paper frame and the pull-out test was performed using a dynamic mechanical analyzer (Q800, TA Instruments) with a displacement rate of 10 μm/min. At the onset of micro-droplet debonding, a maximum force (F_d) was recorded. Usually IFSS can be calculated by

$$\text{IFSS} = \frac{F_d}{\pi D_f L_e} \quad (2)$$

where D_f is the fiber diameter and $\pi D_f L_e$ is the embedded area of the resin on the fiber. Here, IFSS was determined from the slope of the linear regression line in a plot of F_d versus $\pi D_f L_e$, due to the scattering of experimental data [27].

SBS was measured based on an ASTM D2344 standard method using a universal tensile machine (5882, Instron) with a load cell of 100 kN and an average value was determined from six different samples for an each different coating sample.

2.6. Characterization

The zeta potential of the manufactured ANF solution was measured by using an Electrophoretic Light Scattering Spectrophotometer (ELS-8000, Otsuka Electronics). The absorbance of ANF solution before and after EPD was measured by an ultraviolet–visible (UV–Vis) spectroscopy (Cary 5000, Agilent Technologies) at 335 nm wavelength. Chemical structures of a carbon fiber, ANFs, and ANF-coated carbon fibers were studied by Fourier transform infrared (FT-IR) spectroscopy (Nicolet iS10, Thermo Scientific). The micro-structure and size of ANFs were observed using a transmission electron microscopy (TEM, JEOL-2100) with an accelerating voltage of 200 kV. The ANF-coating morphology and crack patterns in the fractured composite samples were investigated by the scanning electron microscopy (SEM, JEOL JSM-5800) observation.

3. Results and discussion

Highly uniform ANFs were prepared by dissolving Kevlar bundles using potassium hydroxide based on the well-established procedure by Yang et al. with slight modification [17]. Prepared ANFs were well-dispersed to form a homogeneous orange-colored solution in DMSO (Fig. 1a). The light-colored observation is due to lower concentration (0.05 wt%) than that in the previous work (0.2 wt%) [17]. A transmission electron microscopy (TEM) image shows individually decomposed ANFs having a diameter of approximately 20 nm with a length of 5–10 μm (Fig. 1b). ANFs had high electrical mobility with a zeta potential value of −18.8 mV, which can promote facile coating on substrates in EPD with a highly dispersive characteristic. Fig. 2 shows a characteristic UV/vis absorbance of ANFs with increasing the concentration of ANF solutions. The highly linear fitting of the absorbance at 335 nm with the ANF concentrations gave a linear equation following the Beer–Lambert law.

In EPD, four different initial concentrations (C_i) of ANF solutions were considered (Table 1). Fourteen carbon fabrics, which are needed for one composite sample, and fifteen steel plates were sequentially connected to corresponding electrodes in an alternating order (Fig. 1), so that ANFs can be well-coated on both sides of carbon fabrics. The amount of coated ANFs in carbon fibers can be quantitatively determined by using the linear equation in Fig. 3, since the difference of the absorbance of ANF solutions before and after EPD can give the concentration of the coated ANF (ΔC). After EPD, the decreases of the concentration for different ANF solutions were almost identical by 2.5%, which implies that the amount of coated ANFs is dominantly dependent on EPD process conditions.

Here an applied voltage and time were fixed as 5 V and 1 min. Note that lower voltage and shorter time gave no significant coating of ANFs, while higher voltage and longer time caused non-uniform and excessive coatings (see Fig. S1 in Supporting Information). The voltage and process time are important parameter to determine the morphology and the amount of coated ANFs. As the voltage and the time in the EPD process increase, the amount of coated ANFs also increases and then reaches a plateau over certain EPD conditions (see Fig. S2 in Supporting Information). Even though higher values of voltage and time than the predetermined conditions of 5 V and 1 min can give higher loading of ANFs, it is hard to obtain well-coated morphology of ANFs on individual carbon fibers. Therefore, the optimum EPD condition can be predetermined to obtain the ideal coating morphology and the amount of ANFs on carbon fibers, although they cannot give kinetically equilibrium.

With known parameters such as the total amount of ANF solution in EPD (M, 3850 g), the areal density of a carbon fabric (d_A, 22 mg/cm^2), the number of fabrics (N, 14 sheets), and the area of EPD coating (A, 64 cm^2), the weight fraction of coated ANFs (C_{ANF}) on a carbon fiber can be calculated by using an analytic equation,

$$C_{ANF} = \frac{M \cdot \Delta C}{d_A \cdot N \cdot A}. \quad (3)$$

Since $\Delta C = 0.025C_i$, the weight fraction of the coated ANFs on a carbon fiber after EPD becomes $C_{ANF} = 4.9C_i$, which were listed in Table 1. As being shown later, 2.5×10^{-2} wt% ANF-coated carbon fiber sample (ANF2) showed the best result on SBS. Note that such content is much less than the value (0.1–5.0 wt%) ever reported for nanofiller hybrid composites exhibiting similar enhancement of SBS (or interlaminar strength) [12,28–31].

The chemical structures of a carbon fiber, ANFs, and ANF-coated carbon fibers (ANF2) were identified by FT-IR spectroscopy, as shown in Fig. 4. The characteristic bands of a pristine ANF at 1649 cm^{-1} (C═O stretching), 1545 cm^{-1} (N—H deformation and C—N stretching), 1516 cm^{-1} (C═C stretching), and 1319 cm^{-1} (Ph—N vibrations) were also observed in the peak of ANF-coated carbon fibers. These observations demonstrate that ANFs are successfully coated on the surface of carbon fibers. The existence of ANFs on a carbon fiber can be also confirmed by a SEM image (see Fig. S3a in Supporting Information). Because ANFs easily construct a thin coating layer after finishing EPD process, we per-

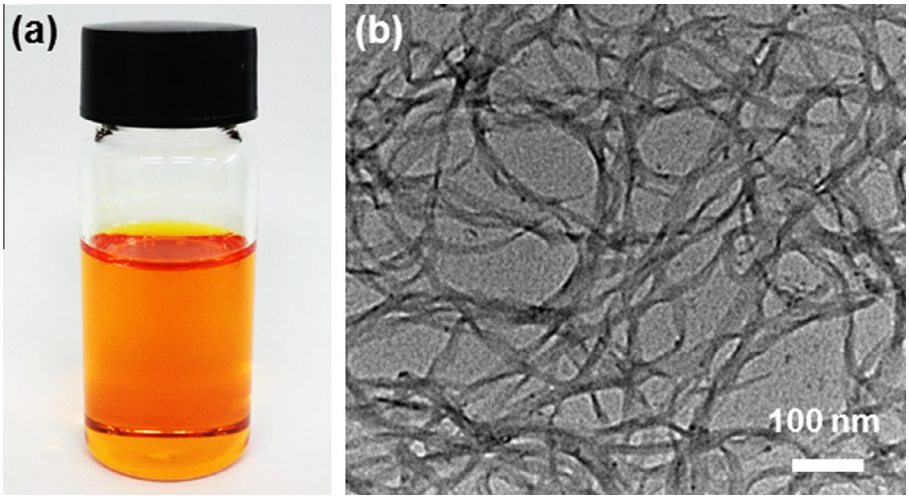

Fig. 2. (a) A photograph of a suspension and (b) a TEM image of ANFs in DMSO. (For interpretation of the references to color in this figure legend, the reader is referred to the web version of this article.)

Table 1
Concentrations of ANF solutions before EPD and weight fractions of coated ANFs on a carbon fiber after EPD.

Notation	Concentration or weight fraction (wt%)	
	Before EPD (C_i in solution)	After EPD (C_{ANF} in fiber)
ANF0	Pristine carbon fiber	
ANF1	1.0×10^{-3}	4.9×10^{-3}
ANF2	5.0×10^{-3}	2.5×10^{-2}
ANF3	1.0×10^{-2}	4.9×10^{-2}
ANF4	5.0×10^{-2}	2.5×10^{-1}

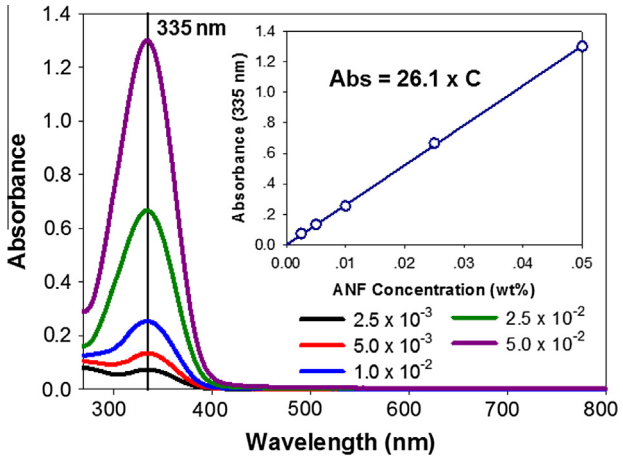

Fig. 3. UV/vis spectra of ANF in DMSO. The inset shows the linear relationship between the absorbance at 335 nm and ANF concentration. (For interpretation of the references to color in this figure legend, the reader is referred to the web version of this article.)

formed a short-time EPD (5 V and 10 sec) for ANF2 concentration. In the figure, a single ANF on a carbon fiber can be clearly seen.

In order to determine the optimum concentration of initial ANF solutions, ANF-coated morphologies on carbon fibers were examined by investigating whether carbon fibers are individually coated with ANFs and the amount of coated ANFs is not too less or excessive. It is because when the amount of coated ANFs is too low, there will be no significant effect on enhancing the mechanical property of carbon fiber composites. When the coating amount is too excessive, it may block micro-channels in a fiber bundle by forming a

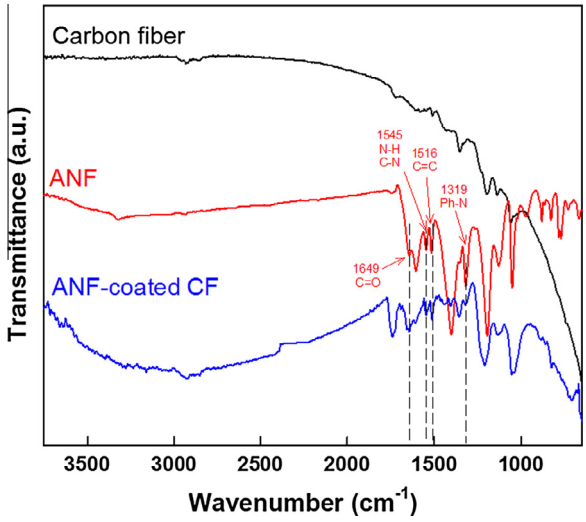

Fig. 4. FT-IR spectra of ANFs, carbon fibers, and ANF-coated carbon fibers (ANF2). (For interpretation of the references to color in this figure legend, the reader is referred to the web version of this article.)

barrier-layer to prevent the complete filling of matrix resin in the composite [9,32]. Fig. 5 shows SEM images of carbon fiber morphologies from different coating cases. Fig. 5a shows a pristine carbon fiber without coating of ANFs. By using 1.0×10^{-3} wt% of ANF concentration (ANF1), the negligible amount of ANFs was observed on carbon fiber (Fig. 5b) where the surface morphology is almost the same as pristine carbon fibers. The ANF2 showed uniform morphologies with individual coating of ANFs (Fig. 5c and d). ANF3 (Fig. 5e) showed thicker and smoother ANF-coating morphology than ANF2 but some ANFs constructed a film across carbon fibers. When a high concentration of ANF was applied (ANF4), a huge and thick ANF-film was formed with covering the entire area of carbon fibers due to excessive deposition (Fig. 5f). Such a covering film of ANFs would lead unhealthy composites with numerous microvoids by obstructing smooth resin infiltration. As for ANF4, a single carbon fiber was detached from neighboring fibers and its SEM image shows that ANFs were not coated on the whole area of the carbon fiber (see Fig. S3b in Supporting Information).

To evaluate the surface properties of ANF-coated carbon fibers, the SFE of each modified carbon fiber was measured based

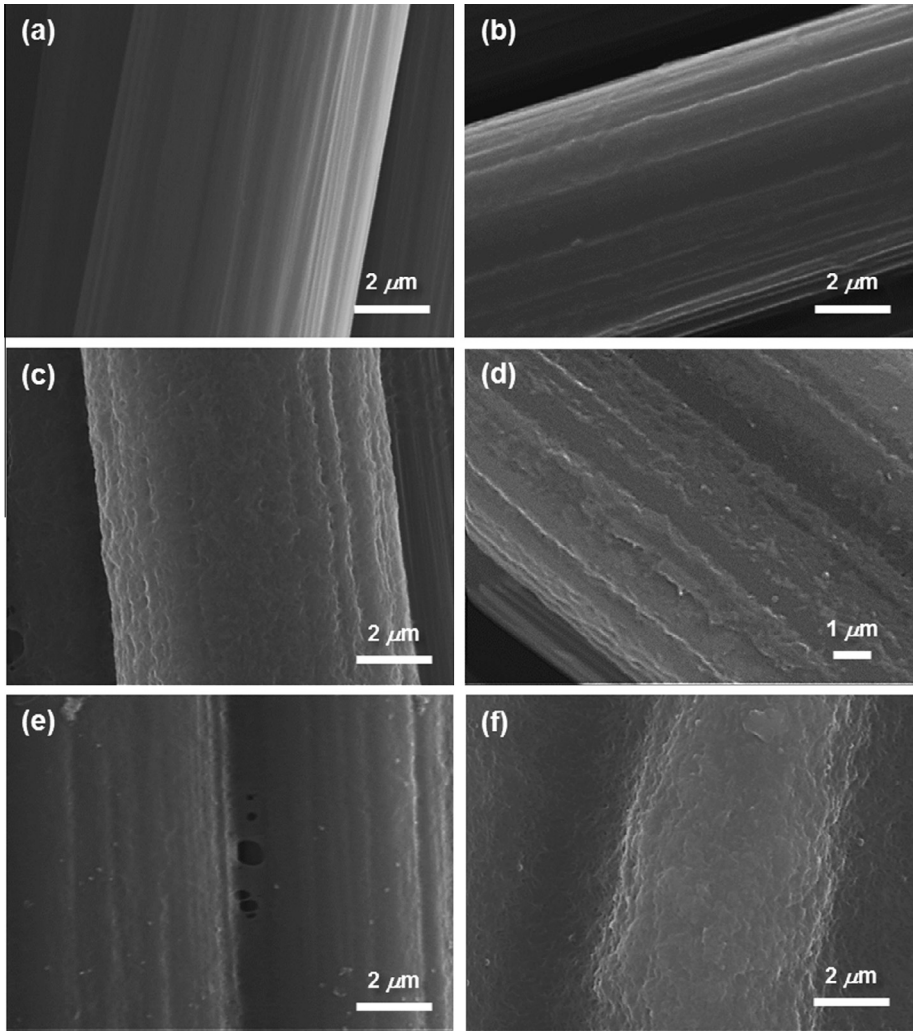

Fig. 5. SEM images of ANF-coated carbon fibers: (a) ANF0, (b) ANF1, (c) ANF2, (d) a magnification of ANF2, (e) ANF3, and (f) ANF4.

on the Owens–Wendt method [25], as shown in Fig. 6a. Specifically, the SFE of the modified carbon fiber was calculated by measuring the contact angle with distilled water and diiodomethane to account for the contribution of the dispersive and polar parts of the SFE, respectively. ANF1 showed negligible increase of the SFE compared with the non-coated carbon fiber, owing to the small amount of ANF-coating. With a slight increase of 2.3% in the polar part of the SFE, ANF2 showed a significant increase of 72.0% in the dispersive part (39.7% in total SFE) compared with the pristine carbon fiber whose SFE was 22.1 and 13.2 mN/m for the dispersive and polar parts, respectively. This can be explained that the abundant aromatic segment and amide groups in the ANF could contribute to the improvement of the dispersive part of the SFE with preserving the polar part, and led to higher total surface energy. Note that ANF3 and ANF4 did not show noticeable increase of SFE despite of the excessive coating of ANFs. This indicates that the coating layer of ANF from 2.5×10^{-2} wt% solution in carbon fibers can be regarded as an optimum loading and is sufficient for enhancing the work of adhesion of carbon fibers.

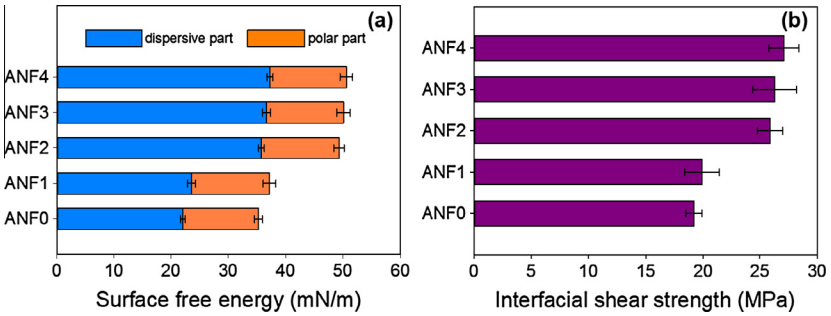

Fig. 6. (a) SFE and (b) IFSS of ANF-coated carbon fibers with different loading amounts. (For interpretation of the references to color in this figure legend, the reader is referred to the web version of this article.)

Table 2
SFE and IFSS of ANF-coated carbon fibers, and SBS of composites.

Sample	SFE (mN/m)			IFSS & SBS (MPa)	
	Polar	Dispersive	Total	IFSS	SBS
ANF0	13.2 (±0.4)	22.1 (±0.3)	35.3 (±0.7)	19.2 (±0.7)	63.7 (±1.5)
ANF1	13.6 (±0.7)	23.6 (±0.6)	37.2 (±1.1)	19.9 (±1.5)	62.3 (±3.5)
ANF2	13.5 (±0.5)	35.8 (±0.4)	49.3 (±0.9)	25.9 (±1.1)	74.5 (±2.3)
ANF3	12.9 (±0.7)	37.2 (±0.5)	50.1 (±1.2)	26.3 (±1.9)	66.9 (±2.9)
ANF4	13.3 (±0.5)	37.3 (±0.6)	50.6 (±1.1)	27.1 (±1.3)	45.1 (±4.6)

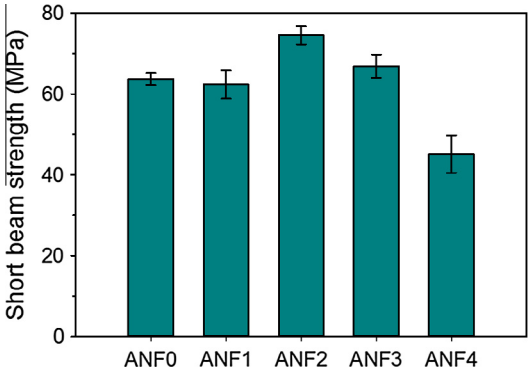

Fig. 7. SBS of ANF-coated carbon fiber composites. (For interpretation of the references to color in this figure legend, the reader is referred to the web version of this article.)

The interfacial adhesion between the ANF-coated carbon fibers and epoxy resin was examined by investigating the IFSS using a micro-droplet pull-out test [26]. From the plots of the maximum debonding force versus the embedded area of micro-droplets of the epoxy matrix, the slope of linear regression lines can give the value of IFSS [27]. Fig. 6b shows that the IFSS of all ANF-coated carbon fibers increased in comparison with that of a pristine carbon fiber (19.2 MPa), and these enhancement well correlates with those in the SFE as summarized in Table 2. While ANF1 showed only 3.6% increase in IFSS, ANF2 exhibited a 34.9% higher IFSS (25.9 MPa) than that of a pristine carbon fiber. Interestingly, IFSS values of ANF3 and ANF4 reached a plateau as observed similarly in the SFE. Thus, the increases in IFSS are dominantly attributed to the higher SFE of the surfaces of the ANF-coated carbon fibers as well as the remarkable mechanical property of the ANFs. Furthermore, the abundant carboxylic acids and amine functional groups could provide many reactive anchoring site for helping the crosslinking and curing the epoxy resin [22,33,34]. Therefore, the surface modification with ANFs can lead to the enhancement of both SFE and IFSS of carbon fibers.

Finally, the effectiveness of the enhanced SFE and IFSS by introducing ANFs on the matrix-dominant mechanical property of carbon fiber reinforced composites was investigated by evaluating the SBS through short-beam shear tests (ASTM D2344). Fig. 7 and Table 2 show that ANF2 exhibited the highest SBS increased by 17.0% because the adequate amount of ANFs was coated on the carbon fiber surface, while the low amount of ANF-coating (ANF1) insignificantly changed SBS. An ANF3 sample has lower SBS than the one of ANF2 owing to smoother surface roughness to hamper a mechanically interlocked structure between the fiber and matrix as well as several ANF-films across each carbon fiber to decelerate the infiltration flow of resin. The smoother fiber surface in ANF3 also reduced the effectiveness of the surface groove in an original pristine carbon fiber, which is beneficial to facilitate the interfacial strength. The SBS in the ANF4 sample largely decreased by 29.2% compared to the ANF0. This huge degradation is because of the thick ANF-film spanning over the carbon fibers, which prevents the smooth resin infiltration into micro-spaces in a yarn and leaves many resin-unfilled voids in a composite sample. Thus, an external load cannot effectively transfer from a matrix to reinforcing fibers and an initiated crack propagates in between a fiber bundle not along the interface between the fiber and matrix. Finally, such a layered composite is delaminated at a low force level. This phenomenon can be easily observed by a fracture pattern in an intra-bundle area (see Fig. S4 in Supporting Information).

To ensure this argument, we measured the weight of epoxy resin in the manufactured composites by subtracting the weight of carbon fibers from the weight of as-produced composites. As for the ANF0 composite, the fiber volume fraction was measured as 51.6% which is similar to the theoretical value 51.9%, and the measured weight of the epoxy resin was 11.3 g (theoretical value is 11.2 g). ANF1 and ANF2 samples showed almost same values

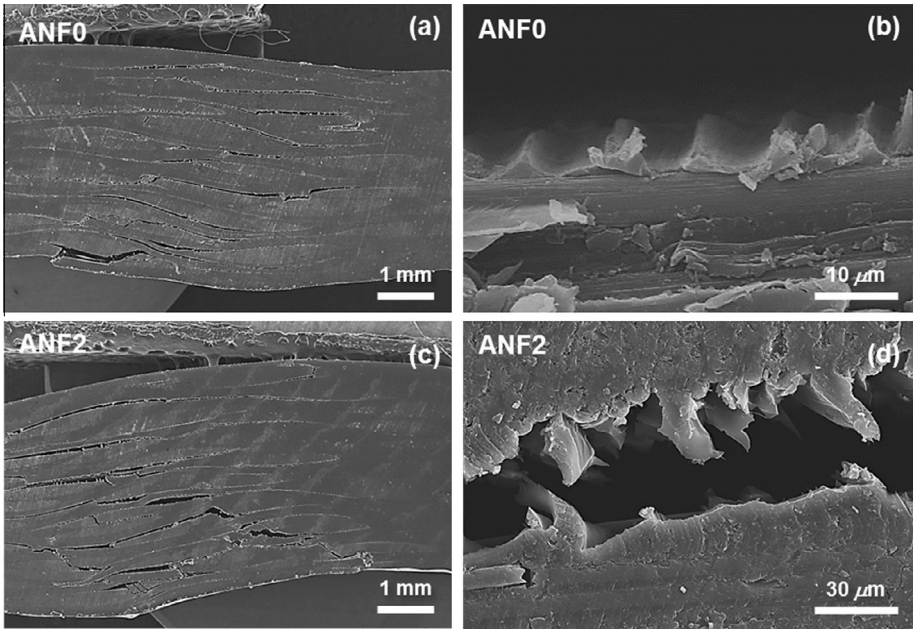

Fig. 8. SEM images of crack patterns and fractured surfaces of pristine ((a) and (b)) and ANF-coated ((c) and (d)) carbon fiber composites.

of resin weight (11.3 and 11.2 g). However ANF3 and ANF4 had lower resin weight of 10.7 and 10.1 g, which represents that the matrix fraction are only 46.1% and 43.5%. Note that the ideal volume fraction of epoxy resin in the composite is 48.4%. Therefore, due to the poor resin infiltration by ANF-films across each carbon fiber, ANF3 and ANF4 had insufficient amount of polymer resin and finally produced unhealthy composites. This suggests that the increase of SFE and IFSS of carbon fibers by the surface modification with ANFs cannot solely determine the enhancement of SBS of the composite. By optimizing the coating amount of ANFs, both the surface roughness and the individually-coated morphology in modified fibers should also be well-controlled in order to accomplish an ultimate increase in SBS.

After evaluation of the load transfer of ANF containing samples, the crack patterns and the fractured surfaces were examined under SEM (Fig. 8). The pristine carbon fiber composite showed cracks in a resin rich region and a laminate interface (Fig. 8a). Also, clear fracture morphology indicates that fibers were readily detached from a matrix due to low mechanical resistance, which represents a low interfacial adhesion (Fig. 8b). However, the ANF2 sample showed many detoured-cracks (Fig. 8c), which implies that coated-ANFs effectively suppressed and delayed the initiation and propagation of cracks. Also, numerous fiber breakages can explain that an applied load was efficiently transferred to the carbon fibers. On the fractured surface in ANF2 (Fig. 8d), many epoxy debris were still adhered, which confirms the strong interfacial bonding between the ANF-coated carbon fiber and the epoxy matrix.

4. Conclusions

We successfully coated ANFs on carbon fibers using a simple but effective EPD with facile morphology control by varying initial concentration of ANF in order to enhance the interfacial adhesion between the carbon fiber and the epoxy matrix. The EPD with optimized process parameters facilitated the development of individually ANF-coated carbon fibers having increased interfacial properties and controlled surface morphology. Particularly, the increase of SFE, IFSS, and SBS was mainly attributed to the abundant functionalities and the outstanding mechanical properties of ANFs. The enhancement of SBS also depends on the surface roughness of ANF-coated fibers and the configuration in a fiber bundle. Noticeably, with remarkably low embedding amount of ANFs (only 0.025 wt%), the interfacial adhesion of carbon fibers was effectively enhanced. Therefore, ANF-coating with fine-controlled surface morphology using a facile EPD can offer a novel sizing tool for an advanced fiber composites. Furthermore, ANFs can be applied for polymer nanocomposites as innovating fillers due to their superior mechanical performance and solution-processability.

Acknowledgements

This work was supported by the National Research Foundation of Korea (NRF) grant funded by the Korea government (MSIP) (No. 2015R1A2A2A04003160) and was also supported by the Industrial Technology Innovation Program (No. 1004338) by the Ministry of Trade, Industry & Energy (Korea).

Appendix A. Supplementary material

Supplementary data associated with this article can be found, in the online version, at http://dx.doi.org/10.1016/j.compositesa.2016.02.029.

References

[1] Mouritz AP, Bannister MK, Falzon PJ, Leong KH. Review of applications for advanced three-dimensional fibre textile composites. Compos Part A – Appl Sci Manuf 1999;30(12):1445–61.
[2] Guades E, Aravinthan T, Islam M, Manalo A. A review on the driving performance of FRP composite piles. Compos Struct 2012;94(6):1932–42.
[3] Benmokrane B, Wang P, Ton-That TM, Rahman H, Robert JF. Durability of glass fiber-reinforced polymer reinforcing bars in concrete environment. J Compos Constr 2002;6(3):143–53.
[4] Taraghi I, Fereidoon A, Taheri-Behrooz F. Low-velocity impact response of woven Kevlar/epoxy laminated composites reinforced with multi-walled carbon nanotubes at ambient and low temperatures. Mater Des 2014;53:152–8.
[5] Kim JK, Mai YW. High strength, high fracture toughness fibre composites with interface control-a review. Compos Sci Technol 1991;41(4):333–78.
[6] George J, Sreekala MS, Thomas S. A review on interface modification and characterization of natural fiber reinforced plastic composites. Polym Eng Sci 2001;41(9):1471–85.
[7] Thomason JL, Yang L. Temperature dependence of the interfacial shear strength in glass–fibre epoxy composites. Compos Sci Technol 2014;96:7–12.
[8] Thostenson ET, Li WZ, Wang DZ, Ren ZF, Chou TW. Carbon nanotube/carbon fiber hybrid multiscale composites. J Appl Phys 2002;91(9):6034–7.
[9] Lee W, Lee JU, Cha HJ, Byun JH. Partially reduced graphene oxide as a multifunctional sizing agent for carbon fiber composites by electrophoretic deposition. RSC Adv 2013;3(48):25609–13.
[10] Lin Y, Ehlert G, Sodano HA. Increased interface strength in carbon fiber composites through a ZnO nanowire Interphase. Adv Funct Mater 2009;19(16):2654–60.
[11] Godara A, Gorbatikh L, Kalinka G, Warrier A, Rochez O, Mezzo L, et al. Interfacial shear strength of a glass fiber/epoxy bonding in composites modified with carbon nanotubes. Compos Sci Technol 2010;70(9):1346–52.
[12] Zhang X, Fan X, Yan C, Li H, Zhu Y, Li X, et al. Interfacial microstructure and properties of carbon fiber composites modified with graphene oxide. ACS Appl Mater Interfaces 2012;4(3):1543–52.
[13] Qian H, Greenhalgh ES, Shaffer MSP, Bismarck A. Carbon nanotube-based hierarchical composites: a review. J Mater Chem 2010;20(23):4751–62.
[14] Nakanishi W, Minami K, Shrestha LK, Ji Q, Hill JP, Ariga K. Bioactive nanocarbon assemblies: nanoarchitectonics and applications. Nano Today 2014;9(3):378–94.
[15] Mukherjee M, Das CK, Kharitonov AP, Banik K, Mennig G, Chung TN. Properties of syndiotactic polystyrene composites with surface modified short Kevlar fiber. Mater Sci Eng, A 2006;441(1–2):206–14.
[16] Hashimoto A, Satoh M, Iwasaki T, Morita M. Fibrillation of aramid fiber using a vibrating ball mill and evaluation of the degree of fibrillation. J Mater Sci 2002;37(18):4013–7.
[17] Yang M, Cao K, Sui L, Qi Y, Zhu J, Waas A, et al. Dispersions of aramid nanofibers: a new nanoscale building block. ACS Nano 2011;5(9):6945–54.
[18] Fan J, Shi Z, Zhang L, Wang J, Yin J. Aramid nanofiber-functionalized graphene nanosheets for polymer reinforcement. Nanoscale 2012;4(22):7046–55.
[19] Fan J, Shi Z, Tian M, Yin J. Graphene–aramid nanofiber nanocomposite paper with high mechanical and electrical performance. RSC Adv 2013;3(39):17664–7.
[20] Fan J, Wang J, Shi Z, Yu S, Yin J. Kevlar nanofiber-functionalized multiwalled carbon nanotubes for polymer reinforcement. Mater Chem Phys 2013;141(2–3):861–8.
[21] Lian M, Fan J, Shi Z, Li H, Yin J. Kevlar®-functionalized graphene nanoribbon for polymer reinforcement. Polymer 2014;55(10):2578–87.
[22] Park B, Lee W, Lee E, Min SH, Kim BS. Highly tunable interfacial adhesion of glass fiber by hybrid multilayers of graphene oxide and aramid nanofiber. ACS Appl Mater Interfaces 2015;7(5):3329–34.
[23] Boccaccini AR, Cho J, Roether JA, Thomas BJC, Minay EJ, Shaffer MSP. Electrophoretic deposition of carbon nanotubes. Carbon 2006;44(15):3149–60.
[24] Besra L, Liu MA. Review on fundamentals and applications of electrophoretic deposition (EPD). Prog Mater Sci 2007;52(1):1–61.
[25] Owens DK, Wendt RC. Estimation of the surface free energy of polymers. J Appl Polym Sci 1969;13(8):1741–7.
[26] Miller B, Muri P, Rebenfeld LA. Microbond method for determination of the shear-strength of a fiber-resin interface. Compos Sci Technol 1987;28(1):17–32.
[27] Zu M, Li Q, Zhu Y, Dey M, Wang G, Lu W, et al. The effective interfacial shear strength of carbon nanotube fibers in an epoxy matrix characterized by a microdroplet test. Carbon 2012;50(3):1271–9.
[28] Galan U, Lin Y, Ehlert GJ, Sodano HA. Effect of ZnO nanowire morphology on the interfacial strength of nanowire coated carbon fibers. Compos Sci Technol 2011;71(7):946–54.
[29] Fan Z, Santare MH, Advani SG. Interlaminar shear strength of glass fiber reinforced epoxy composites enhanced with multi-walled carbon nanotubes. Compos Part A – Appl Sci Manuf 2008;39(3):540–54.
[30] Feng L, Li K, Si Z, Song Q, Li H, Lu J, et al. Compressive and interlaminar shear properties of carbon/carbon composite laminates reinforced with carbon nanotube-grafted carbon fibers produced by injection chemical vapor deposition. Mater Sci Eng, A 2015;626:449–57.

[31] Liu Y, Yang JP, Xiao HM, Qu CB, Feng QP, Fu SY, et al. Role of matrix modification on interlaminar shear strength of glass fibre/epoxy composites. Compos Part B – Eng 2012;43(1):95–8.
[32] Lee W, Lee JU, Byun JH. Catecholamine polymers as surface modifiers for enhancing interfacial strength of fiber-reinforced composites. Compos Sci Technol 2015;110:53–61.
[33] Kang S, Hong SI, Choe CR, Park M, Rim S, Kim J. Preparation and characterization of epoxy composites filled with functionalized nanosilica particles obtained via sol–gel process. Polymer 2001;42(3):879–87.
[34] Zhu J, Wei S, Ryu J, Budhathoki M, Liang G, Guo Z. In situ stabilized carbon nanofiber (CNF) reinforced epoxy nanocomposites. J Mater Chem 2010;20(23):4937–48.